Depletion of nonlinearity in magnetohydrodynamic turbulence: Insights from analysis and simulations

J. D. Gibbon, A. Gupta, G. Krstulovic, R. Pandit, H. Politano, Y. Ponty, A. Pouquet, G. Sahoo, and J. Stawarz

Depletion of Nonlinearity in Magnetohydrodynamic Turbulence: Insights from Analysis and Simulations

J. D. Gibbon[1], A. Gupta[2], G. Krstulovic[3], R. Pandit[4], H. Politano[5], Y. Ponty[3], A. Pouquet[6,7], G. Sahoo[2], and J. Stawarz[7]

[1]*Department of Mathematics, Imperial College London, London SW7 2AZ, UK.*
[2]*Department of Physics, University of Rome 'Tor Vergata', 00133 Roma, Italy.*
[3]*Laboratoire Lagrange, Université Côte d'Azur, Observatoire de la Côte d'Azur,*
CNRS, Blvd de l'Observatoire, CS 34229, 06304 Nice cedex 4, France.
[4]*Centre for Condensed Matter Theory, Indian Institute of Science, Bangalore, 560 012, India.*
[5]*Laboratoire Dieudonné, Université de Nice Sophia-Antipolis, France.*
[6]*National Center for Atmospheric Research,*
P.O. Box 3000, Boulder, CO 80307, USA.
[7]*Laboratory for Atmospheric and Space Physics,*
University of Colorado, Boulder, CO 80303, USA.

It is shown how suitably scaled, order-m moments, $D_m^\pm$, of the Elsässer vorticity fields in three-dimensional magnetohydrodynamics (MHD) can be used to identify three possible regimes for solutions of the MHD equations with magnetic Prandtl number $P_M = 1$. These vorticity fields are defined by $\boldsymbol{\omega}^\pm = \mathrm{curl}\, \boldsymbol{z}^\pm = \boldsymbol{\omega} \pm \boldsymbol{j}$, where $\boldsymbol{z}^\pm$ are Elsässer variables, and where $\boldsymbol{\omega}$ and $\boldsymbol{j}$ are, respectively, the fluid vorticity and current density. This study follows recent developments in the study of three-dimensional Navier-Stokes fluid turbulence [Gibbon *et al.* Nonlinearity 27, 2605 (2014)]. Our mathematical results are then compared with those from a variety of direct numerical simulations (DNSs) which demonstrate that all solutions that have been investigated remain in *only one of these regimes* which has depleted nonlinearity. The exponents $q^\pm$ that characterize the inertial range power-law dependencies of the $\boldsymbol{z}^\pm$ energy spectra, $\mathcal{E}^\pm(k)$, are then examined, and bounds are obtained. Comments are also made on: (a) the generalization of our results to the case $P_M \neq 1$ and (b) the relation between $D_m^\pm$ and the order-m moments of gradients of magnetohydrodynamic fields, which are used to characterize intermittency in turbulent flows.

PACS numbers: 47.27.Ak, 52.30.Cv, 47.27.ek, 02.30.Jr

I. INTRODUCTION

Intermittency is widespread in nature: its characterization is a central problem in turbulence [1–9], in nonequilibrium statistical mechanics, in the production and storage of wind and solar energy, and the behaviors of market crashes, and of several critical phenomena [10, 11]. It has also been studied extensively in fluid turbulence [1, 3–9] and in magnetohydrodynamic (MHD) turbulence [12–17], often by using order-p structure functions of fields such as the velocity and, in MHD, the magnetic field. An example is the (longitudinal) velocity ($\boldsymbol{u}$) structure function,

$$\begin{aligned} S_p(r) &\equiv \langle [\delta u(r)]^p \rangle, \\ \delta u(r) &\equiv [\boldsymbol{u}(\boldsymbol{x} + \boldsymbol{r}) - \boldsymbol{u}(\boldsymbol{x})] \cdot \hat{\boldsymbol{r}}, \end{aligned} \quad (1)$$

which scales as

$$S_p(r) \sim r^{\zeta_p} \quad (2)$$

for $\eta_d \ll r \ll L$, where η_d is the dissipation length scale below which viscous dissipation is significant, L is the large length scale at which energy is injected into the fluid, and the multiscaling exponents ζ_p, which are nonlinear, monotone increasing functions of p, characterize the intermittency [1]. Simple scaling is obtained if ζ_p depends linearly on p, as in the phenomenological approach (K41) of Kolmogorov [18].

To determine ζ_p is a challenging task [5, 6, 9], which is especially difficult for time-dependent structure functions [19, 20] or MHD turbulence [12–17]. Therefore, we explore other signatures of intermittency. For three-dimensional (3D) fluid turbulence Refs. [21–23] have introduced a new way of analyzing direct numerical simulations (DNSs) to obtain fresh insights into suitably scaled (see below), order-m moments D_m of the vorticity $\boldsymbol{\omega} = \nabla \times \boldsymbol{u}$. These studies show the following: (a) on theoretical grounds, three regimes, I, II, and III, are possible, with the D_m ordered in different ways

(Fig. 1, Ref. [23]); but (b) *only regime I is observed in a wide variety of DNSs* [22, 23]. Regime I has sufficiently depleted nonlinearity so that a global attractor exists, provided the solutions remain in this region, as they do in all the DNSs examined so far from this point of view.

The analog of the above theoretical framework is developed for the case of 3D MHD turbulence. Then the behaviors of $D_m^\pm$ are examined – the 3D MHD counterparts of D_m in [22, 23] – in a variety of DNSs, which have been carried out independently by different groups, to obtain new insights into the depletion of nonlinearity here. It is found that 3D MHD turbulence is like its fluid-turbulence counterpart inasmuch as all solutions remain in *only one regime, with depleted nonlinearity, in a large variety of DNSs*. The implications of our results are also examined for the exponents $q^\pm$ that characterize the power-law inertial range dependencies of the energy spectra $\mathcal{E}^\pm(k)$ of the Elsässer variables on the wave number k.

The remainder of this paper is organized as follows. In §II the MHD equations are introduced and our numerical methods are summarized. §III contains the mathematical analysis of these equations. §IV is devoted to the energy spectra that emerge from these calculations. §V contains the principal conclusions of the paper. The technical details of some of our calculations have been relegated to Appendices A, B and C.

II. MODEL AND NUMERICAL METHODS

A. The equations in Elsässer variables

The velocity $\boldsymbol{u}$ and magnetic field $\boldsymbol{b}$ can be combined into the Elsässer variables

$$z^\pm = \boldsymbol{u} \pm \boldsymbol{b}\,. \qquad (3)$$

Then the incompressible 3D MHD equations are

$$(\partial_t + \boldsymbol{z}^\mp \cdot \nabla)\boldsymbol{z}^\pm \;=\; \nu_+\nabla^2\boldsymbol{z}^\pm + \nu_-\nabla^2\boldsymbol{z}^\mp$$
$$- \;\nabla\mathcal{P} + \boldsymbol{f}^\pm\,, \qquad (4)$$

where $\nabla \cdot \boldsymbol{z}^\pm = 0$, $\mathcal{P}$ is the total pressure, $\nu_\pm = \frac{1}{2}(\nu \pm \eta)$, and ν and η are, respectively, the kinematic viscosity and the magnetic diffusivity, whose ratio yields the magnetic Prandtl number $P_M = \nu/\eta$. The two forcing functions, $\boldsymbol{f}^\pm(\boldsymbol{x})$, are defined by

$$\boldsymbol{f}^\pm(\boldsymbol{x}) = \boldsymbol{f}_u \pm \boldsymbol{f}_b\,. \qquad (5)$$

which are absent in decaying MHD turbulence. $\boldsymbol{j} = \nabla \times \boldsymbol{b}$ is the current density. The mean magnetic field $\boldsymbol{B}_0$ in zero in our simulations. The following notation will be used for spatial and temporal averages:

$$\langle \cdot \rangle_V = L^{-3}\int_{\mathcal{V}} \cdot\, dV\,, \qquad (6)$$

$$\langle \cdot \rangle_T = T^{-1}\int_0^T \cdot\, dt\,, \qquad (7)$$

with the L^2-spatial norm represented by

$$\| \cdot \|_2 = \left(\int_{\mathcal{V}} |\cdot|^2\, dV\right)^{1/2}\,. \qquad (8)$$

The Taylor-microscale Reynolds number R_Λ is defined as

$$R_\Lambda = u_{rms}\nu^{-1}\left(\frac{\langle \boldsymbol{u}^2 + \boldsymbol{b}^2\rangle_V}{\langle \boldsymbol{\omega}^2 + \boldsymbol{j}^2\rangle_V}\right)^{1/2}\,, \qquad (9)$$

with u_{rms} the root-mean-square velocity. Our DNSs of the 3D MHD equations use a periodic cubic box and a pseudo-spectral method [12–16] with large-scale initial conditions, and in some cases, forcing (Table I). All our numerical simulations are fully de-aliased.

For ideal 3D MHD (i.e., $\nu_\pm = 0$, $\boldsymbol{f}^\pm = 0$) the invariants are the energies

$$E_\pm = \tfrac{1}{2}\langle \boldsymbol{z}_\pm \cdot \boldsymbol{z}_\pm\rangle_V = E_T \pm H_C \qquad (10)$$

together with the magnetic and cross helicities

$$H_M = \langle \boldsymbol{A} \cdot \boldsymbol{b}\rangle_V\,, \qquad H_C = \langle \boldsymbol{u} \cdot \boldsymbol{b}\rangle_V\,, \qquad (11)$$

where the vector potential $\boldsymbol{A}$ is related to $\boldsymbol{b}$ by

$$\boldsymbol{b} = \nabla \times \boldsymbol{A}\,, \qquad (12)$$

and the total energy is

$$E_T \;=\; \tfrac{1}{2}\langle \boldsymbol{u}\cdot\boldsymbol{u} + \boldsymbol{b}\cdot\boldsymbol{b}\rangle_V$$
$$=\; E_u + E_b\,. \qquad (13)$$

The relative rates of cross and magnetic and cross helicity are also defined as

$$\sigma_m = \cos(\boldsymbol{A}, \boldsymbol{b})\,, \qquad \sigma_C = \cos(\boldsymbol{u}, \boldsymbol{b})\,, \qquad (14)$$

with $|\sigma_{c,m}| \le 1$. These represent the degree to which the fields are aligned and they are also measures, global or point-wise, of the strength of nonlinearities in MHD.

By defining the two combinations of the vorticity and the current as

$$\boldsymbol{\omega}^\pm = \boldsymbol{\omega} \pm \boldsymbol{j}\,, \qquad (15)$$

it is shown in Appendix A that $\boldsymbol{\omega}^\pm$ evolve according to (with $P_M = 1$)

$$(\partial_t + \boldsymbol{z}^\mp \cdot \nabla)\boldsymbol{\omega}^\pm - \boldsymbol{\omega}^\mp \cdot \nabla \boldsymbol{z}^\pm - \nu\Delta\boldsymbol{\omega}^\pm \qquad (16)$$

$$= \boldsymbol{\omega}^\mp \times \boldsymbol{\omega}^\pm + \sum_{i=1}^{3} \partial_i \boldsymbol{z}^\pm \times \partial_i \boldsymbol{z}^\mp + \nabla \times \boldsymbol{f}^\pm\,.$$

The two terms on the right-hand side stem from the equation for the current; the labels $i = 1, 2$, and 3 refer, respectively, to x, y, and z.

In the ideal case, the constraints that follow from conservation laws involve mixed $(\boldsymbol{u}, \boldsymbol{b})$ correlators [24, 25]. In the absence of a strong uniform magnetic field $\boldsymbol{B}_0$, magnetic fluctuations at a scale comparable to that of the system, $\boldsymbol{B}_L$, play a role equivalent to that of $\boldsymbol{B}_0$ for the small scales, provided there is sufficient scale separation, i.e., for high-Reynolds-number flows. It has been argued in [14] that measurable anisotropy develops for scales smaller than the Taylor scale based on $\boldsymbol{B}_L$. Therefore, the inertial-range energy spectrum can be of either Kolmogorov (K41) or Iroshnikov-Kraichnan (IK) forms, depending on the cross correlation. Dimensional analysis gives

$$\zeta_p^{IK} = p/4\,, \qquad (17)$$

if the model of Iroshnikov and Kraichnan (IK) [26, 27] is used and $\sigma_C = 0$; or

$$\zeta_p^{K41} = p/3\,, \qquad (18)$$

if K41 [16, 18] is used. Appendix B discusses some of these scaling arguments in a phenomenonogical manner. Moreover,

$$\mathcal{E}^\pm(k) \sim \begin{cases} k^{-3/2} & (IK) \\ k^{-5/3} & (K41)\,. \end{cases} \qquad (19)$$

III. MATHEMATICAL ANALYSIS

The generalization of the analysis of Refs. [22, 23] for the 3D NS equations is now described in the case of the 3D MHD equations. The relevant partial differential equations (PDEs) in Elsässer variables are (4) and (16). Two spatially and tem-

Some models [28, 29] and DNS results [16, 30, 31] indicate that the departure from linear scaling, be it of the IK or K41 forms, is stronger in 3D MHD turbulence than in 3D Navier-Stokes (NS) turbulence, which suggests a depletion of nonlinearity by virtue of the tendency of alignment or anti-alignment of $\boldsymbol{u}$ and $\boldsymbol{b}$ [32, 33].

B. Description of runs

Table I contains the parameters for the runs analyzed in this paper. All runs have been performed in three dimensions by using periodic boundary conditions, no imposed external magnetic field and a magnetic Prandtl number P_M of unity, except for the pm-runs; no modeling of the small scales is employed. For the sd-runs (spin-down) the Reynolds number is varied. The initial condition for the spin-down runs sd is the three-dimensional Orszag-Tang vortex [34], with added phase shifts to set $\sigma_C \simeq -0.21$ initially. The Aa-Ae runs are high-resolution forced runs [35, 36], with a constant velocity and magnetic forcing for which all the modes in the first two Fourier shells are kept constant. From the Aa to Ae runs, the resolution increases with the Reynolds number. The tg-runs are forced in both the velocity and induction equations. In these runs, the four-fold symmetries of the Taylor-Green vortex extended to MHD are implemented. Moreover, the three runs have different resulting energy spectra (IK, K41, and k^{-2}), although they have the same ideal invariants but with different cross-correlations [37]. Finally, the pm runs have a fixed viscosity, but variable magnetic diffusivities and thus allow for extending the analysis to the case of $P_M \neq 1$ (see [16]).

porally averaged velocities, $U^\pm$, based on $\boldsymbol{z}^\pm$, are defined as

$$U^{\pm 2} = L^{-3} \left\langle \|\boldsymbol{z}^\pm\|_2^2 \right\rangle_T\,. \qquad (20)$$

In turn, the $U^\pm$ allow us to define two Reynolds numbers

$$Re_\pm = LU^\pm/\nu\,. \qquad (21)$$

TABLE I: Parameters for our direct numerical simulations. $k_{\max} = N/3$ is the maximum resolved wavenumber at grid resolution N (the standard 2/3 de-aliasing rule). Λ_T and R_Λ are defined in (9). σ_C and σ_M are the relative rates of cross-helicity and magnetic helicity, respectively. $\lambda^\pm$ are the parameters extracted from the data for high m (subscript max) and low m (subscript min) (See Fig.2, column 3).

Run	N	R_Λ	Λ_T	P_M	σ_C	σ_M	$\lambda^+_{\min}$	$\lambda^+_{\max}$	$\lambda^-_{\min}$	$\lambda^-_{\max}$
sd1	128	14	0.27	1	-0.27	-0.22	1.096	1.158	1.101	1.169
sd2	256	21	0.20	1	-0.27	-0.23	1.103	1.165	1.116	1.186
sd3	512	30	0.15	1	-0.27	-0.24	1.111	1.171	1.129	1.197
sd4	768	45	0.11	1	-0.26	-0.24	1.121	1.184	1.141	1.206
Aa	512	35	0.098	1	0.019	0.003	1.049	1.150	1.049	1.156
Ab	1024	54	0.074	1	0.017	0.004	1.057	1.197	1.060	1.195
Ac	2048	120	0.036	1	0.011	Data Not Available	1.076	1.167	1.076	1.176
Ad	2048	161	0.027	1	0.009	Data Not Available	1.074	1.168	1.073	1.157
Ae	4096	341	0.014	1	0.010	Data Not Available	1.070	1.163	1.072	1.174
tgi	1024	100	0.066	1	0	0	1.121	1.196	1.117	1.197
tga	1024	83	0.084	1	0	0	1.161	1.202	1.138	1.202
tgc	1024	110	0.056	1	~ 0.05	0	1.084	1.183	1.089	1.175
pm01	512	240	0.14	0.1	0.122	0.0047	1.078	1.238	1.078	1.234
pm02	512	140	0.10	1.0	0.075	0.0049	1.070	1.171	1.069	1.160
pm03	512	80	0.06	10	0.226	0.0077	1.053	1.149	1.052	1.158

The Reynolds numbers are based on average velocities, while two Grashof numbers $Gr_\pm$ are based on the forcing functions $\boldsymbol{f}^\pm(\boldsymbol{x})$, namely,

$$Gr_\pm = L^{3/2}\|\boldsymbol{f}^\pm\|_2/\nu^2 . \qquad (22)$$

For the class of forcing functions spectrally concentrated around a single length-scale ($\ell = L$ for the purposes of this paper), a relation exists between $Gr_\pm$ and $Re_\pm$ for solutions of (4) that has been derived through the method of Doering-Foias [38] (see Appendix C) where it has been shown that

$$Gr_\pm \leq c\, Re_\pm\, (Re_\mp + 1) , \qquad Gr_\pm \gg 1 . \quad (23)$$

The main variables used in this paper are L^{2m}-norms of the vorticity field, defined in such a way that each has the dimension of a frequency:

$$\Omega^\pm_m(t) = \left(L^{-3} \int_{\mathcal{V}} |\boldsymbol{\omega}^\pm|^{2m} dV \right)^{1/2m} . \qquad (24)$$

By Hölder's inequality, the $\Omega^\pm_m$ are naturally ordered such that

$$\Omega^\pm_1 \leq \Omega^\pm_m \leq \Omega^\pm_{m+1} . \qquad (25)$$

If a signal has no intermittency, then the $\Omega^\pm_m$ will be packed close together, whereas a strongly intermittent signal will cause them to spread out widely. The following scaling was first introduced in work on the 3D Navier-Stokes equations [21–23] and will be followed here:

$$D^\pm_m = \left(\varpi_0^{-1} \Omega^\pm_m \right)^{\alpha_m} , \qquad (26)$$

where the exponent α_m is defined as

$$\alpha_m = \frac{2m}{4m - 3} , \qquad (27)$$

and where $\varpi_0 = \nu L^{-2}$ is the box frequency. The α_m-scaling comes from symmetry considerations. The ordering of the $\Omega^\pm_m$ in (25) does not necessarily hold for the $D^\pm_m$ as α_m is decreasing with respect to m. The $D^\pm_m$ are the main variables to be used. Under the assumption that (4) has a solution we now look at the evolution of $D^\pm_1$:

$$\tfrac{1}{2}\varpi_0^{-1}\dot{D}_1^{\pm} \;\leq\; -L^{-1}\varpi_0^{-2}\int_{\mathcal{V}}|\nabla\boldsymbol{\omega}^{\pm}|^2 dV + L^{-3}\varpi_0^{-3}\int_{\mathcal{V}}\left|\boldsymbol{\omega}^{\pm}\cdot\left(\boldsymbol{\omega}^{\mp}\cdot\nabla\boldsymbol{z}^{\pm}\right)\right|dV$$

$$+\; L^{-3}\varpi_0^{-3}\sum_{i=1}^{3}\int_{\mathcal{V}}\left|\boldsymbol{\omega}^{\pm}\cdot\left(\partial_i\boldsymbol{z}^{\pm}\times\partial_i\boldsymbol{z}^{\mp}\right)\right|dV + Gr_{\pm}D_1^{\pm 1/2}. \tag{28}$$

To estimate the first nonlinear term in (28) we write ($1 < m < \infty$)

$$\int_{\mathcal{V}}\left|\boldsymbol{\omega}^{\pm}\cdot\left(\boldsymbol{\omega}^{\mp}\cdot\nabla\boldsymbol{z}^{\pm}\right)\right|dV \;\leq\; \int_{\mathcal{V}}\left|\boldsymbol{\omega}^{\pm}\right|^{\frac{2m-3}{2(m-1)}}\left|\boldsymbol{\omega}^{\pm}\right|^{\frac{1}{2(m-1)}}\left|\boldsymbol{\omega}^{\mp}\right|^{\frac{2m-3}{2(m-1)}}\left|\boldsymbol{\omega}^{\mp}\right|^{\frac{1}{2(m-1)}}\left|\nabla\boldsymbol{z}^{\pm}\right|dV$$

$$\leq\; c_{1,m}\left(\int_{\mathcal{V}}|\boldsymbol{\omega}^{\pm}|^2\,dV\right)^{\frac{2m-3}{4(m-1)}}\left(\int_{\mathcal{V}}|\boldsymbol{\omega}^{\pm}|^{2m}\,dV\right)^{\frac{1}{4m(m-1)}} \tag{29}$$

$$\times\;\left(\int_{\mathcal{V}}|\boldsymbol{\omega}^{\mp}|^2\,dV\right)^{\frac{2m-3}{4(m-1)}}\left(\int_{\mathcal{V}}|\boldsymbol{\omega}^{\mp}|^{2m}\,dV\right)^{\frac{1}{4m(m-1)}}\left(\int_{\mathcal{V}}|\boldsymbol{\omega}^{\pm}|^{2m}\,dV\right)^{1/2m}.$$

Note that the sum of the five exponents in the latter expression is unity. For the last term we have invoked the inequality[49], which requires a Riesz transform in its proof, namely ,

$$\|\nabla\boldsymbol{z}^{\pm}\|_{2m}\leq c_{2,m}\|\boldsymbol{\omega}^{\pm}\|_{2m}\,, \tag{30}$$

provided $1\leq m<\infty$. Then (29) becomes

$$L^{-3}\varpi_0^{-3}\int_{\mathcal{V}}\left|\boldsymbol{\omega}^{\pm}\cdot\left(\boldsymbol{\omega}^{\mp}\cdot\nabla\boldsymbol{z}^{\pm}\right)\right|dV \;\leq\; c_{3,m}\left[D_1^{\pm}\right]^{\frac{2m-3}{4(m-1)}}\left[D_m^{\pm}\right]^{\frac{1}{2\alpha_m(m-1)}}$$

$$\times\;\left[D_1^{\mp}\right]^{\frac{2m-3}{4(m-1)}}\left[D_m^{\mp}\right]^{\frac{1}{2\alpha_m(m-1)}}\left[D_m^{\pm}\right]^{\frac{1}{\alpha_m}}.$$

$$\leq\; c_{3,m}\left[D_1^{\pm}\right]^{\frac{2m-3}{4(m-1)}}\left[D_m^{\pm}\right]^{\frac{2m-1}{2\alpha_m(m-1)}}$$

$$\times\;\left[D_1^{\mp}\right]^{\frac{2m-3}{4(m-1)}}\left[D_1^{\mp}\right]^{\frac{1}{2\alpha_m(m-1)}}. \tag{31}$$

As in the 3D Navier-Stokes equations, this estimate of the nonlinearity is too strong for the dissipation terms. However, what was observed in computations of the 3D Navier-Stokes equations is that it displays numerically much weaker behavior than the estimate equivalent to (31) [23]. This can be measured by numerically tracking D_m in terms of D_1, the equivalent of which for 3D MHD is[50] :

$$D_m^{\pm}\leq\left[D_1^{\pm}\right]^{A_{m,\lambda}^{\pm}}\,, \tag{32}$$

where, for $2\leq m\leq 9$, $A_{m,\lambda}^{\pm}$ is defined as

$$A_{m,\lambda}^{\pm}=\frac{m\lambda^{\pm}+1-\lambda^{\pm}}{4m-3}. \tag{33}$$

In effect, $\lambda^{\pm}$ is a fitting parameter for the maxima in time. An explanation why such a relation should hold can be found in [39]. The range of values of $\lambda^{\pm}$ have been determined numerically (see Fig. 2 and Table I). By inserting (32) into (31) it is found that

$$L^{-3}\varpi_0^{-3}\int_{\mathcal{V}}\left|\boldsymbol{\omega}^{\pm}\cdot\left(\boldsymbol{\omega}^{\mp}\cdot\nabla\boldsymbol{z}^{\pm}\right)\right|dV \;\leq\; c_{4,m}\left[D_1^{\pm}\right]^{\frac{\chi_m^{\pm}(2m-1)+m(2m-3)}{4m(m-1)}}\left[D_1^{\mp}\right]^{\frac{\chi_m^{\mp}+m(2m-3)}{4m(m-1)}}. \tag{34}$$

Next, the second nonlinear term in (28) is considered where (30) is used. From this, it is found that the estimate for the right-hand side of (34) is the same as in (29), apart from the constant $c_{5,m}$:

$$\sum_{i=1}^{3}\int_{\mathcal{V}}\left|\boldsymbol{\omega}^{\pm}\cdot\left(\partial_i\boldsymbol{z}^{\pm}\times\partial_i\boldsymbol{z}^{\mp}\right)\right|dV \;\leq\; c_{5,m}\left(\int_{\mathcal{V}}|\boldsymbol{\omega}^{\pm}|^2\right)^{\frac{2m-3}{4(m-1)}}\left(\int_{\mathcal{V}}|\boldsymbol{\omega}^{\pm}|^{2m}\right)^{\frac{1}{4m(m-1)}} \tag{35}$$

$$\times\;\left(\int_{\mathcal{V}}|\boldsymbol{\omega}^{\mp}|^2\right)^{\frac{2m-3}{4(m-1)}}\left(\int_{\mathcal{V}}|\boldsymbol{\omega}^{\mp}|^{2m}\right)^{\frac{1}{4m(m-1)}}\left(\int_{\mathcal{V}}|\boldsymbol{\omega}^{\pm}|^{2m}\right)^{1/2m}.$$

Converting this into the $D_m^\pm$ gives the same right-hand side as in (34) but with a constant $c_{2,m}$. Taking all these terms together, (28) becomes

$$\tfrac{1}{2}\varpi_0^{-1}\dot{D}_1^\pm \leq -L^{-1}\varpi_0^{-2}\int_{\mathcal{V}}|\nabla\boldsymbol{\omega}^\pm|^2 dV + c_{6,m}\left[D_1^\pm\right]^{\frac{\chi_m^\pm(2m-1)+m(2m-3)}{4m(m-1)}}\left[D_1^\mp\right]^{\frac{\chi_m^\mp+m(2m-3)}{4m(m-1)}} + Gr_\pm D_1^{\pm 1/2}\,. \quad (36)$$

To handle the coupled nature of the $\pm$-variables we define

$$X = D_1^\pm + D_1^\mp \qquad \text{and} \qquad E_0 = \max_t\left(E^+, E^-\right) \quad (37)$$

and the two bounded dimensionless energies are defined by $E^\pm = \nu^{-2}L^{-1}\int_{\mathcal{V}}|\boldsymbol{z}^\pm|^2\,dV$. By adding the $\pm$-equations and using the depletion formulae (32) and (33), a differential inequality is found for $X(t)$

$$\tfrac{1}{2}\varpi_0^{-1}\dot{X} \leq -\frac{X^2}{2E_0} + c_{6,m}X^{1+\frac{1}{2}\lambda^\pm-(\lambda^\pm-\lambda^\mp)/4m} + 2\max\left(Gr_+, Gr_-\right)X^{1/2}\,. \quad (38)$$

Note that when $\lambda^\pm = \lambda^\mp = \lambda$, as in the Navier-Stokes case, then the exponent of the nonlinear term reduces to $1 + \tfrac{1}{2}\lambda$, as it should.

Without the use of the numerically observed depletion in (32), standard methods in analysis leads to a term $\propto X^3$ in Eq.(38) (see Ref. [23] for the NS case), which does not lead to a control over the solutions at large times. However, provided $\lambda^\pm$ and $\lambda^\mp$ satisfy

$$1 + \tfrac{1}{2}\lambda^\pm - \frac{(\lambda^\pm - \lambda^\mp)}{4m} < 2, \quad (39)$$

an 'absorbing ball' for X exists because E_0 is bounded above. This ball has finite radius (depending on the upper bound on E_0) into which solutions are drawn if initial conditions are set outside the ball, and which cannot escape if initial conditions are set inside. (39) can be rewritten as

$$\lambda^\pm < 2 + \epsilon_m^\pm, \quad (40)$$

where $\epsilon_m^\pm = (\lambda^\pm - \lambda^\mp)/2m$, which is a small number. Subject to the constraints on $\lambda^\pm$ in (40), the ball is such that the $\boldsymbol{z}^\pm$ are L^2-bounded, and thus so are $\boldsymbol{u}$ and $\boldsymbol{b}$. Additionally, the control of X that (38) affords (an H_1-bound) is also enough to prove its compactness. This ball is thus the global attractor which governs the long-time dynamics of the PDEs.

The *natural*, 3D-MHD analogs of Fig. 1 in Ref. [23] are the schematic plots of D_m^+ versus D_1^+ and D_m^- versus D_1^- in Fig. 1, which show three regimes. For regular solutions, we must have

$$1 \leq \lambda^\pm \leq 2 + \epsilon^\pm\,, \qquad \text{(regime I)}\,. \quad (41)$$

The $\epsilon^\pm$-term has been left off the figure as it is small and can take either sign. When

$$2 + \epsilon^\pm \leq \lambda^\pm < 4\,, \qquad \text{(regime II)} \quad (42)$$

there is depletion, but not enough to control solutions; and, finally, when

$$\lambda_\pm \geq 4\,, \qquad \text{(regime III)} \quad (43)$$

then $D_m^\pm \geq c_m D_1^\pm$. However, any initial data set in this region would be pathological as it would have to be prepared as a very large spike in $\boldsymbol{\omega}^\pm$ in which the L^∞-norm is much larger than the L^2-norm. In the NS-case, it can be shown that solutions are regular in regime III, but no more than algebraically increasing because of the forcing [39]. *Our DNS*
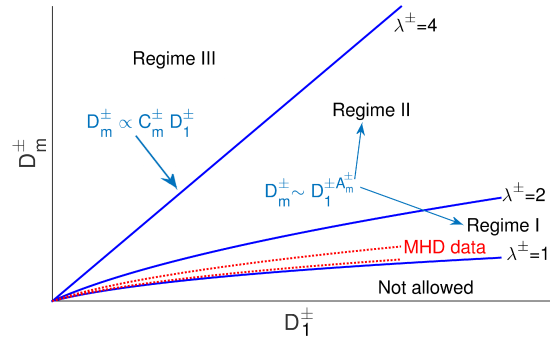

FIG. 1: (Color online) Schematic plots of $D_m^\pm$ versus $D_1^\pm$ showing the three regimes in 3D MHD (see text). The additive term $\epsilon^\pm$ in (41) has been omitted because it is small and can take either sign. The values of $\lambda^\pm$ in Table I lie only just above the lower bound $\lambda^\pm = 1$. Solutions are regular in regime I but not in regime II. To start in regime III requires unphysical initial data.

data indicate that regime I ($1 \leq \lambda^\pm \leq 2 + \epsilon^\pm$) is obtained in 3D MHD for all the solutions we have studied.

In Fig. 2 representative results from four of our DNSs are given. The first column of Fig. 2 contains log-log (base 10) plots of the energy spectra $E(k)$ versus k. Most of these energy spectra show power-law forms in the inertial range with an exponent that is consistent with the K41 value $-5/3$. However, this exponent is consistent with the IK value $-3/2$ for run-tgc; and it is -2 for run-tgi. We find that these exponents can depend on the values of σ_C and σ_M, which are given in Table I.

The second column of Fig. 2 has plots of $A_m^+(t)$ versus t, from which $A_{m,\lambda}^+$ is determined (plots for $A_m^-(t)$ versus t are similar), which follow from $D_m^+(t)$. The region where the data lie do not follow exactly the contour boundary curves of Fig. 1. The $\lambda^\pm$ have been determined as in Ref. [23] for the 3D-NS equations. $\lambda_m^\pm$ are defined to be those values that have been computed from Eq. (33) for $A_{m,\lambda}^\pm$. A check has shown that our data are reliable up to $m = 10$; note the ordering of the $A_{m,\lambda}^\pm$ is the same for all our runs.

In the third column of Fig. 2, plots of $\lambda_m^\pm$ versus m are given, in the range $2 \leq m \leq 9$, for which good-quality numerical data have been obtained. From these plots $\lambda^\pm$ has been found from the minimum over m of $\lambda_m^\pm$. In general, $1 \leq \lambda_\pm \leq 4$; however, in all our DNSs, $1 \leq \lambda_\pm \leq 2$, i.e., our solutions lie in regime I.

IV. SPECTRA

A. How to estimate the spectrum for the 3D MHD-Elsässer system

The method of Doering and Gibbon [40] is now followed which explains how to estimate average length scales and a corresponding spectrum based on ideas in [1]. It is necessary to define a set of time-averaged inverse length scales[51]

$$\left\langle L^2 \kappa_{2,1}^{\pm 2} \right\rangle_T = \left\langle \frac{L^2 \|\nabla \boldsymbol{\omega}^\pm\|_2^2 dV}{\|\boldsymbol{\omega}^\pm\|_2^2} \right\rangle_T = \left\langle \frac{L^{-1} \varpi_0^{-2} \int_\mathcal{V} |\nabla \boldsymbol{\omega}^\pm|^2 dV}{D_1^\pm} \right\rangle_T, \quad (44)$$

where the labelling of the subscripts is based on the number of derivatives on $\boldsymbol{z}^\pm$. Dividing (36) by $D_1^\pm$ and time averaging, we find[52]

$$\left\langle L^2 \kappa_{2,1}^{\pm 2} \right\rangle_T \leq c_{6,m} \left\langle \left[D_1^\pm\right]^{\frac{(\chi_m^\pm - m)(2m-1)}{4m(m-1)}} \left[D_1^\mp\right]^{\frac{\chi_m^\mp + m(2m-3)}{4m(m-1)}} \right\rangle_T$$

$$\leq c_{6,m} \left\langle D_1^\pm \right\rangle_T^{\frac{(\chi_m^\pm - m)(2m-1)}{4m(m-1)}} \left\langle D_1^\pm \right\rangle_T^{\frac{\chi_m^\mp + m(2m-3)}{4m(m-1)}}. \quad (45)$$

Secondly, it is necessary to estimate $\left\langle D_1^\pm \right\rangle_T$ by using the energy inequality version of (4)

$$\tfrac{1}{2}\frac{d}{dt}\|\boldsymbol{z}^\pm\|_2^2 \leq -\nu\|\boldsymbol{\omega}^\pm\|_2^2 + \|\boldsymbol{z}^\pm\|_2\|\boldsymbol{f}^\pm\|_2. \quad (46)$$

By time averaging, converting into a dimensionless form, and using (23), it is found that

$$\left\langle D_1^\pm \right\rangle_T \leq Gr_\pm Re_\pm \leq c\, Re_\pm^2\,(Re_\mp + 1). \quad (47)$$

Moreover, by introducing the definitions, the first of which is the Elsässer analog of the Taylor microscale,

$$\kappa_{1,0}^{\pm 2} = \frac{\|\boldsymbol{\omega}^\pm\|_2^2}{\|\boldsymbol{z}^\pm\|_2^2}, \qquad \kappa_{2,0}^{\pm 4} = \frac{\|\nabla\boldsymbol{\omega}^\pm\|_2^2}{\|\boldsymbol{z}^\pm\|_2^2}, \quad (48)$$

and adapting ideas in [40], (46) gives

$$\left\langle L^2 \kappa_{1,0}^{\pm 2} \right\rangle_T \leq Re_\pm. \quad (49)$$

Then it is easily shown that

$$\left\langle L\kappa_{2,0}^\pm \right\rangle_T \leq \left\langle L^2 \kappa_{2,1}^{\pm 2} \right\rangle_T^{1/4} \left\langle L^2 \kappa_{1,0}^{\pm 2} \right\rangle_T^{1/4}, \quad (50)$$

and so from (44), (49) and (47), in which only the dominant term has been kept, it is found that

$$\left\langle L\kappa_{2,0}^\pm \right\rangle_T \leq c_{6,m} Re_\pm^{\sigma_m^\pm} (Re_\mp + 1)^{\rho_m^\mp}, \quad (51)$$
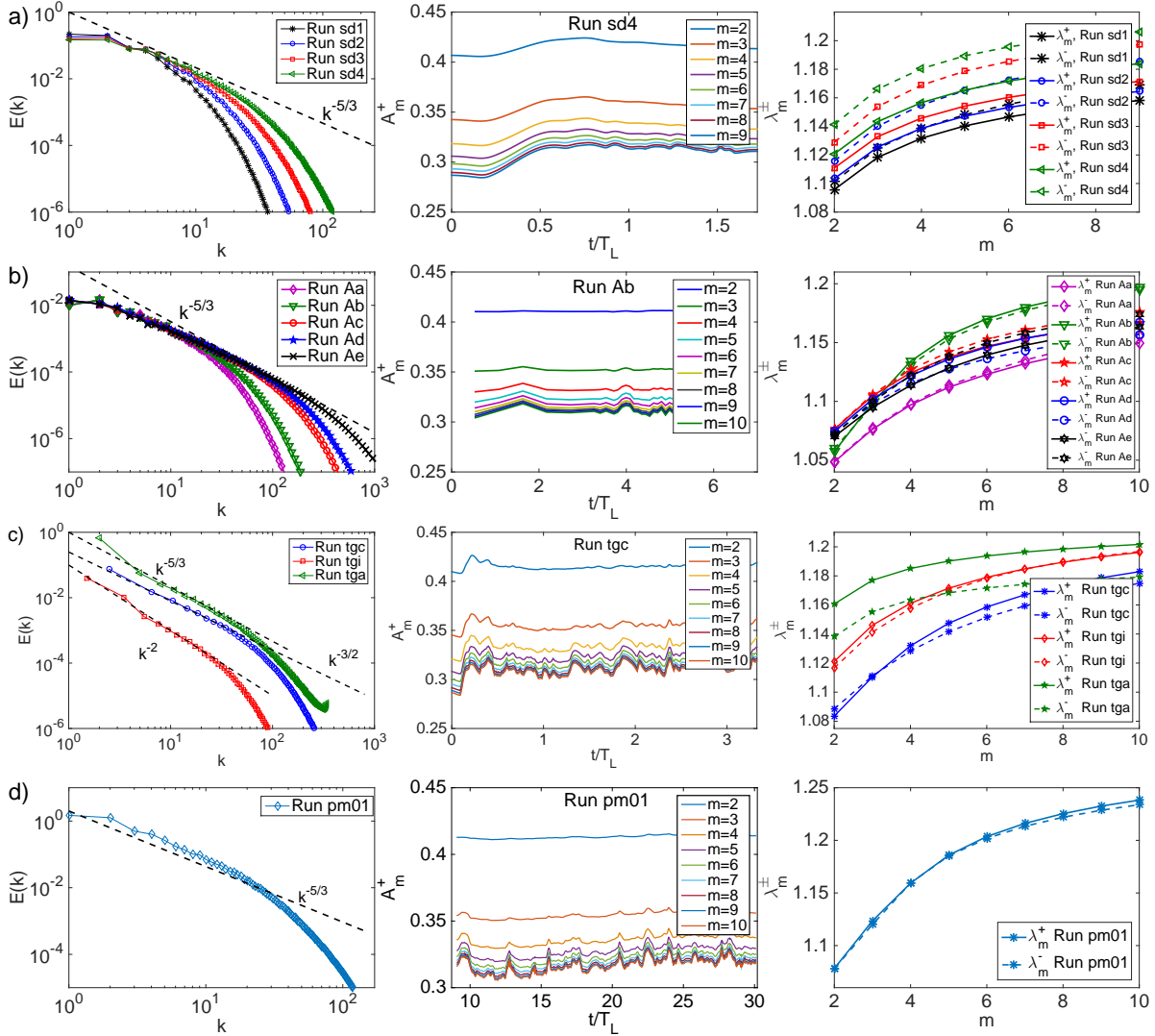
FIG. 2: (Color online) Representative results from our DNSs: total energy spectra (first column), temporal evolution of A_m^+ (second column) and values of $\lambda_m^\pm$ (third column). The rows correspond to different runs: a) decaying 3D MHD turbulence; b) forced, statistically steady 3D MHD turbulence; c) forced, statistically steady 3D MHD turbulence with imposed Taylor-Green symmetries and d) forced, statistically steady 3D MHD turbulence with $P_M = 0.1$. For parameters see Table I.

where, with $\chi_m^\pm = (m-1)\lambda^\pm + 1$,

$$\sigma_m^\pm = \frac{\lambda^\pm + 1}{4} + \left(\frac{\lambda^\mp - \lambda^\pm}{8m}\right), \qquad (52)$$

$$\rho_m^\mp = \frac{(2m-1)\lambda^\mp + \lambda^\pm}{16m}. \qquad (53)$$

Thus, (52) can be written as

$$\left\langle L\kappa_{2,0}^\pm \right\rangle_T \leq c\, Re_\pm^{\frac{\lambda^\pm+1}{4}} Re_\mp^{\frac{\lambda^\mp}{8}}, \qquad (54)$$

where the factor of unity has been ignored in the large $Re^\pm$-limit and the limit of large m has been

taken. Then the problem is whether it is possible to consider Re_+ and Re_- as independent variables or not. The simplest way is to note that

$$\begin{aligned} \|\boldsymbol{z}^\pm\|^2 &\leq \|\boldsymbol{v}\|_2^2 + 2\|\boldsymbol{v}\|_2\|\boldsymbol{b}\|_2 + \|\boldsymbol{b}\|_2^2 \\ &\leq 2\left(\|\boldsymbol{v}\|_2^2 + \|\boldsymbol{b}\|_2^2\right) = 4E_{\text{tot}}. \end{aligned} \qquad (55)$$

Defining a *global* Reynolds number as

$$Re = L\sqrt{2E_{\text{tot}}}/\nu\,, \qquad (56)$$

(54) gives

$$\left\langle L\kappa_{2,0}^\pm \right\rangle_T \leq c\, Re^{\frac{\lambda^\pm+1}{4} + \frac{\lambda^\mp}{8}}. \qquad (57)$$
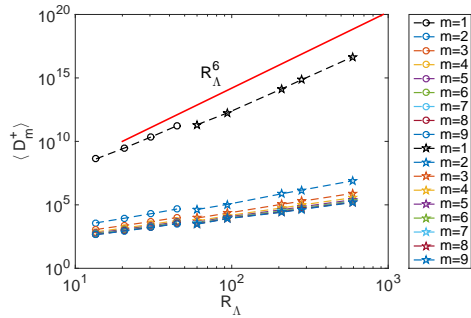
FIG. 3: (Color online) Plots versus R_Λ of $\langle D_m^+ \rangle_{st.av.}$, for the runs Aa-Ae (pentagrams) and its decaying-MHD analog, for the runs sd1-sd4 (circles), where we use the value of D_m^+ at the time at which the energy dissipation rate ϵ reaches its first maximum [16]. See Table I for additional information about these runs.

Now the implications of these results are examined for energy spectra derived in (57). By assuming isotropy and the power-law Ansätze

$$\mathcal{E}^\pm(k) = \begin{cases} A\, k^{-q^\pm}, & L^{-1} \le k \le k_c^\pm, \\ 0, & k > k_c^\pm, \end{cases} \quad (58)$$

the identification (see Appendix B and [1])

$$\langle L\kappa_{2,0}^\pm \rangle_T \sim (L\, k_c^\pm)^{1-\frac{q^\pm-1}{4}} \sim Re^{\frac{5-q}{4(3-q)}}, \quad (59)$$

allows us to find an inequality relation between $q^\pm$ and $\lambda_\pm$.

$$q^\pm \ge 3 - \frac{4}{2\lambda^\pm + \lambda^\mp} \ge \frac{5}{3}, \quad (60)$$

which excludes the IK exponent $3/2$, at least in the absence of intermittency. However, full isotropy has been assumed at all scales and the limit $Re \to \infty$ when comparing (57) and (59). Furthermore, (59) implicitly assumes $E_+ = E_-$. In general, this relation is modified leading to a set of inequalities for the $q^\pm$ that do not exclude IK (last two equations in Appendix B). In fact, IK is excluded *only* if correlation is neglected. This is consistent with the fact that run-tgc (see Fig. 2 and Table I) produces an IK scaling because it has a non-zero cross-correlation. It is known that in the presence of cross correlations between the velocity and magnetic field ($H_C \ne 0$), different indices arise for the energy spectra of the two Elsässer fields, $z^\pm$ (see, e.g., [41] and references therein), a result that persists in the case of weak MHD turbulence, as shown through wave-turbulence developments [42]. The mathematical analysis as well as the numerical simulations presented in this paper, all put

on firm ground that indeed H_C plays a crucial role in determining the distribution of energy among scales.

In Fig. 3 plots of $\langle D_m^+ \rangle_{st.av.}$ versus R_Λ have been displayed, where the angular brackets now indicate the average over the statistically stationary turbulent state; we present data (pentagrams in Fig. 3) from the runs Aa-Ae (Table I). Circles indicate decaying-MHD data points (runs sd1-sd4); here we use the value of D_m^+ at the time at which the energy-dissipation rate ϵ reaches its first maximum [16]. The order-m moments of gradients, or *gradmoments*, of hydrodynamic fields have been used to investigate Nelkin scaling [43–45], i.e., the power-law dependence of the gradmoments on the Reynolds number Re in the case of fluid turbulence; the Nelkin-scaling exponents ξ_m can be related to the structure-function exponents ζ_m [43–45]. Our vorticity moments are upper bounds for gradmoments of the Elsässer variables (see (30)). If these bounds are saturated, then the exponents, which can be extracted from the plots of Fig. 3, should be related to the Nelkin exponents for 3D MHD turbulence. A more detailed exposition of such scaling in 3D MHD has been deferred to another study.

In liquid metals, as well as in the solar photosphere, P_M is very small. It can also be very large as, e.g., in the interstellar medium. Our mathematical analysis is not valid if $P_M \ne 1$ because ν_- can become negative for $P_M \le 1$. However, our DNS results in Fig. 3 show that plots for $P_M = 0.1$ (bottom row) are similar to their counterparts for $P_M = 1$ (top three rows). Furthermore, at least for a fixed value of ν, Table I shows that the values of $\lambda_m^\pm$ are comparable to their $P_M = 1$ counterparts; these values of $\lambda^\pm$ decrease marginally as P_M is increased.

V. CONCLUSIONS

Our work, which builds upon the studies of Refs. [22, 23, 46] for fluid turbulence, provides new insights into the depletion of nonlinearity in 3D MHD turbulence and its intermittency. In particular, we have introduced the scaled moments $D_m^\pm$, and then obtained inequalities containing $D_m^\pm$ and $D_1^\pm$; these inequalities specify three possible regimes. In essence, it has been found that 3D MHD turbulence is similar to its fluid-turbulence counterpart insofar as all solutions that

have been investigated have remained in only one regime (regime I), which displays depleted nonlinearity (Fig. 1). Moreover, under the assumption of isotropy our results lead to the inequality (60) for the spectral exponents $q^{\pm}$. In fact, the inequality (30) can relate $D_m^{\pm}$ and the order-m moments of gradients of the magnetohydrodynamic fields; such moments can then be used, along with a suitable generalization of Nelkin scaling [43–45] for 3D MHD turbulence, to relate slopes of plots like those in Fig. 3 to the multiscaling exponents of Elsässer-field structure functions. We conclude that 3D MHD appears to have more nonlinear depletion than fluid turbulence, because the values of $\lambda^{\pm}$ are lower than those for their fluid-turbulence counterparts; this can be attributed to Alfvén waves weakening the nonlinear eddies.

Acknowledgments

Appendix A: Vorticity and current equations

The following four identities have been used for vectors $\boldsymbol{D}$ and $\boldsymbol{Q}$ (not necessarily divergence-free):

$$
\begin{aligned}
\nabla \times [\nabla \times \boldsymbol{D}] &= \nabla[\nabla \cdot \boldsymbol{D}] - \nabla^2 \boldsymbol{D} \\
\nabla[\boldsymbol{D} \cdot \boldsymbol{Q}] &= \boldsymbol{D} \times [\nabla \times \boldsymbol{Q}] + \boldsymbol{Q} \times [\nabla \times \boldsymbol{D}] \\
&+ \boldsymbol{D} \cdot \nabla \boldsymbol{Q} + \boldsymbol{Q} \cdot \nabla \boldsymbol{D} \\
\nabla \cdot [\boldsymbol{D} \times \boldsymbol{Q}] &= \boldsymbol{Q} \cdot \nabla \times \boldsymbol{D} - \boldsymbol{D} \cdot \nabla \times \boldsymbol{Q} \\
\nabla \times [\boldsymbol{D} \times \boldsymbol{Q}] &= \boldsymbol{Q} \cdot \nabla \boldsymbol{D} - \boldsymbol{D} \cdot \nabla \boldsymbol{Q} .
\end{aligned} \tag{A1}
$$

The equation for the vorticity is derived straightforwardly:

$$
(\partial_t + \boldsymbol{u} \cdot \nabla)\boldsymbol{\omega} = \boldsymbol{\omega} \cdot \nabla \boldsymbol{u} + \boldsymbol{b} \cdot \nabla \boldsymbol{j} - \boldsymbol{j} \cdot \nabla \boldsymbol{b} . \tag{A2}
$$

By using $\boldsymbol{D} = \boldsymbol{u} \times \boldsymbol{b}$ in the above identities (with $\nabla \cdot \boldsymbol{D} \neq 0$), we obtain the equation for the current

$$
\partial_t \boldsymbol{j} = \nabla \left[\nabla \cdot [\boldsymbol{u} \times \boldsymbol{b}] - \nabla^2[\boldsymbol{u} \times \boldsymbol{b}] \right] , \tag{A3}
$$

which, upon expansion, leads to:

$$
\begin{aligned}
\nabla[\nabla \cdot [\boldsymbol{u} \times \boldsymbol{b}]] &= \boldsymbol{\omega} \cdot \nabla \boldsymbol{b} + \boldsymbol{b} \cdot \nabla \boldsymbol{\omega} - \boldsymbol{b} \times \nabla^2 \boldsymbol{u} + \boldsymbol{\omega} \times \boldsymbol{j} - \boldsymbol{u} \cdot \nabla \boldsymbol{j} - \boldsymbol{j} \cdot \nabla \boldsymbol{u} + \boldsymbol{u} \times \nabla^2 \boldsymbol{b} - \boldsymbol{j} \times \boldsymbol{\omega} \quad \text{(A4)} \\
-\nabla^2[\boldsymbol{u} \times \boldsymbol{b}] &= -\nabla^2 \boldsymbol{u} \times \boldsymbol{b} - \boldsymbol{u} \times \nabla^2 \boldsymbol{b} - 2\Sigma_i \partial_i \boldsymbol{u} \times \partial_i \boldsymbol{b} . \quad \text{(A5)}
\end{aligned}
$$

So the equation for the current (note the cancellations in the ∇^2 terms) is:

$$(\partial_t + \boldsymbol{u} \cdot \nabla)\boldsymbol{j} - \boldsymbol{\omega} \cdot \nabla \boldsymbol{b} - \boldsymbol{b} \cdot \nabla \boldsymbol{\omega} + \boldsymbol{j} \cdot \nabla \boldsymbol{u} - 2\boldsymbol{\omega} \times \boldsymbol{j} = -2\Sigma_i \partial_i \boldsymbol{u} \times \partial_i \boldsymbol{b} \,, \tag{A6}$$

an expression already written in [47]. For the curl of the Elsässer field $\boldsymbol{\omega}^+ = \boldsymbol{\omega} + \boldsymbol{j}$, (with $\pm$ symmetry for $\partial_t \boldsymbol{\omega}^-$), (A6) and (A2) reduce to (16)

$$(\partial_t + \boldsymbol{z}^- \cdot \nabla)\boldsymbol{\omega}^+ = \boldsymbol{\omega}^- \cdot \nabla \boldsymbol{z}^+ + \boldsymbol{\omega}^- \times \boldsymbol{\omega}^+ + \Sigma_i \partial_i \boldsymbol{z}^+ \times \partial_i \boldsymbol{z}^- \,. \tag{A7}$$

Note that the geometry term $2\boldsymbol{\omega} \times \boldsymbol{j}$ in the equation for the current density does not appear in the vorticity equation; also, it is weak for almost-aligned current and vorticity (or $\boldsymbol{\omega}^\pm$) [34, 48]. The equations (A7) for the temporal evolution of $\boldsymbol{\omega}^\pm$ follow immediately from the above. Note also that $\boldsymbol{\omega}^- \times \boldsymbol{\omega}^+ = 2\boldsymbol{\omega} \times \boldsymbol{j}$ does not affect the point-wise production of $\boldsymbol{\omega}^\pm$, whereas the second term can create current density; here the labels $i = 1, 2$, and 3 refer respectively to the x, y, and z derivatives. Finally note that, for a flow evolving towards strong local correlations between the velocity and magnetic field ($\boldsymbol{z}^+ = 0$ or $\boldsymbol{z}^- = 0$), this extra term is weak.

Appendix B: Phenomenological argument for fluids and MHD

In the fluid case, the total energy and dissipation can be written in terms of the energy spectrum with spectral index q as

$$U^2 = \int_{k_0}^{k_c} A k^{-q} \,, \qquad \epsilon = \nu \int_{k_0}^{k_c} A k^{2-q} \,, \tag{B1}$$

with the dimension of A as $[A] = [\epsilon^a][L^b]$. One finds straightforwardly $a = 2/3$, $b = [5 - 3q]/3$, so $b = 0$ for $q = 5/3$, as expected. This leads to a cut-off wavenumber $k_c/k_0 = [\epsilon \nu^{-3}]^{1/[3(3-q)]} \, k_0^{-4/[3(3-q)]}$, or in terms of the Reynolds number,

$$Re = UL/\nu = \epsilon^{1/3} L^{4/3} \nu^{-1} \,, \qquad Lk_c = Re^x \,,$$
$$x = [3 - q]^{-1} \,, \tag{B2}$$

with $k_0 = 2\pi/L$.

In MHD, one can follow the weak-turbulence IK prescription (remaining in the isotropic framework for simplicity). Then, $A = [\epsilon B_0]^c L^d$, where B_0 is a large-scale strong (quasi)-uniform magnetic field; so $c = 1/2$, $d = [3 - 2q]/2$. This leads to

$$k_c/k_0 = [\epsilon B_0^{-1} \nu^{-2}]^{1/[2(3-q)]} \, k_0^{-3/[2(3-q)]} \,; \tag{B3}$$

or, in terms of the Reynolds number,

$$Re = UL/\nu = [\epsilon B_0 L^5]^{1/4} \nu^{-1} \,, \tag{B4}$$

with

$$Lk_c = r^x Re^x \,, \qquad x = [3 - q]^{-1} \,,$$
$$r = \frac{U}{B_0} << 1 \,, \tag{B5}$$

which is a hypothesis that is compatible with the wave-turbulence assumption. Thus, with the introduction of the factor r, the scale dependence of the cut-off wavenumber with Reynolds number is the same for fluids and MHD.

This phenomenological argument can be reproduced in the more general case when the velocity and magnetic fields are correlated, i.e., with $E_+ \neq E_-$. This results in a condition between the indices $q_\pm$ of the $E_\pm$ spectra, namely $q_+ + q_- = 3$ within the IK framework with, as before for the uncorrelated flows, $q_+ = q_- = 3/2$ (see [47] for an introduction). Two-point closure computations and two-dimensional numerical simulations find $q_+ \neq q_-$ at high correlations, but the three-dimensional case remains open. As in the preceding case of uncorrected MHD, we make the assumption that the $\pm$ integral scales are both comparable to the box size L.

After some algebra along the same lines as before, one finds that the dissipative wave numbers for the $E_\pm(k)$ spectra are equal both to $k_+ = k_- = k_c = \epsilon/[\nu^2 B_0]^{1/3}$, as in the zero-correlation case, or :

$$Lk_\nu = [z_0^+/B_0]^{1/3} [z_0^-/B_0]^{1/3} Re_+^{1/3} Re_-^{1/3} \,, \tag{B6}$$

with $Re_\pm = z_0^\pm L/\nu$, and we have assumed that the magnetic Prandtl number is equal to unity so that $\nu = \eta = \nu_+ = \nu_-$. Writing

$$E_\pm(k) = A_\pm(\epsilon, B_0, L) k^{-q_\pm} \,,$$
$$A_\pm(\epsilon, B_0, L) = \epsilon^{a_\pm} B_0^{b_\pm} L^{c_\pm} \,, \tag{B7}$$

it is readily found that, under the assumption that

$$b_+ + b_- = -3(a_+ + a_-) + 4 = 1 \qquad \text{(B8)}$$

(so that $E_+(k)E_-(k) \sim [\epsilon B_0]k^{-3}$), and that

$$c_+ + c_- = -3 + (3 - q_+) + (3 - q_-), \qquad \text{(B9)}$$

then

$$Lk_c \sim \frac{\epsilon}{[\nu^2 B_0]}^{\frac{1}{(3-q_+)+(3-q_-)}} L^{\frac{3}{(3-q_+)+(3-q_-)}}, \quad \text{(B10)}$$

or, in terms of the Reynolds numbers $Re_\pm$,

$$Lk_c \sim [[z_0^+/B_0][z_0^-/B_0]]^{\frac{1}{(3-q_+)+(3-q_-)}}$$
$$\times [Re_+ Re_-]^{\frac{1}{(3-q_+)+(3-q_-)}}. \qquad \text{(B11)}$$

Finally, this phenomenological relation can be used as in the non-correlated case to establish the upper bounds of spectral indices. In this case one finds that

$$\frac{[1 - \frac{1}{4}(q_+ - 1)]}{(3 - q_+) + (3 - q_-)} \leq \min\left\{\frac{\lambda_+ + 1}{4} ; \frac{\lambda_-}{8}\right\}, \qquad \text{(B12)}$$

and similarly

$$\frac{[1 - \frac{1}{4}(q_- - 1)]}{(3 - q_+) + (3 - q_-)} \leq \min\left\{\frac{\lambda_- + 1}{4} ; \frac{\lambda_+}{8}\right\}, \qquad \text{(B13)}$$

with $1 < q_\pm < 3$ and $1 + \lambda_\pm/2 < 2$ using equation (40). These results are to be contrasted with the uncorrelated case obtained in the Kolmogorov framework. It is possible to show that in the correlated case the IK spectrum $q_\pm = 3/2$ cannot be excluded.

Appendix C: The Doering-Foias $Gr^\pm - Re^\pm$ relation for MHD

Following Doering and Foias [38] the forcing function $\boldsymbol{f}^\pm(\boldsymbol{x})$ is split into its magnitude $F^\pm$ and its "shape" $\boldsymbol{\phi}^\pm$ such that

$$\boldsymbol{f}^\pm(\boldsymbol{x}) = F^\pm \boldsymbol{\phi}^\pm(\ell^{-1}\boldsymbol{x}), \qquad \text{(C1)}$$

where ℓ is the longest length scale in the force and is taken to be $\ell = L$ for convenience in the rest of the paper. On the unit torus $\mathbb{I}_d$ in d-dimensions, $\boldsymbol{\phi}$ is a mean-zero, divergence-free vector field with the chosen normalization property

$$\int_{\mathbb{I}_d} \left|\nabla_y^{-1}\boldsymbol{\phi}^\pm\right|^2 d^d y = 1. \qquad \text{(C2)}$$

L^2-norms of $\boldsymbol{f}^\pm$ on $\mathbb{I}^d$ are

$$\|\nabla^N \boldsymbol{f}^\pm\|_2^2 = C_N^\pm \ell^{-2N} L^d F^{\pm 2}, \qquad \text{(C3)}$$

where the coefficients $C_N^\pm$, which refer to the shape of the force but not its magnitude, are

$$C_M^\pm = \sum_n |2\pi n|^{2N} |\hat{\boldsymbol{\phi}}_n^\pm|^2. \qquad \text{(C4)}$$

Various bounds exist such as (among others)

$$\|\nabla \Delta^{-M} \boldsymbol{f}^\pm\|_\infty = D_M^\pm F \ell^{2M-1}. \qquad \text{(C5)}$$

The energy dissipation rate ϵ is

$$\epsilon^\pm = \left\langle \nu L^{-d} \int_{\mathcal{V}} |\nabla \boldsymbol{z}^\pm|^2 dV \right\rangle = \nu L^{-d} \left\langle H_1^\pm \right\rangle. \qquad \text{(C6)}$$

In terms of $F^\pm$, the Grashof number in (22) becomes ($\ell = L$)

$$Gr_\pm = F^\pm \ell^3/\nu^2. \qquad \text{(C7)}$$

Following the procedure in [38] (pg 296 equation (2.9)), we multiply (4) by $(-\Delta^{-M})\boldsymbol{f}^\pm$ and integrate to obtain

$$\frac{d}{dt}\int_{\mathbb{I}_d} \boldsymbol{z}^\pm \cdot [(-\Delta^{-M})\boldsymbol{f}^\pm] \, dV = \nu \int_{\mathbb{I}_d} \Delta \boldsymbol{z}^\pm \cdot [(-\Delta^{-M})\boldsymbol{f}^\pm] - \int_{\mathbb{I}_d} \boldsymbol{z}^\mp \cdot \nabla \boldsymbol{z}^\pm \cdot [(-\Delta^{-M})\boldsymbol{f}^\pm] \, dV$$
$$+ \int_{\mathbb{I}_d} \boldsymbol{f}^\pm \cdot [(-\Delta^{-M})\boldsymbol{f}^\pm] \, dV. \qquad \text{(C8)}$$

Now if we integrate all the terms by parts, and take the time average, we get

$$\left\langle L^{-d} \int_{\mathbb{I}_d} \left| \nabla^{-M} \boldsymbol{f}^{\pm} \right|^2 \, dV \right\rangle \; \leq \; \nu \left\langle L^{-d} \int_{\mathbb{I}_d} \left| \boldsymbol{z}^{\pm} \cdot (-\Delta^{-M+1}) \boldsymbol{f}^{\pm} \right| \, dV \right\rangle$$
$$+ \; \left\langle L^{-d} \int_{\mathbb{I}_d} \left| \boldsymbol{z}^{\mp} \cdot [\nabla[(-\Delta^{-M})] \boldsymbol{f}] \cdot \boldsymbol{z}^{\pm} \right| \, dV \right\rangle . \tag{C9}$$

Thus, after a Schwarz inequality, (C9) turns into

$$c_0 F^{\pm 2} \ell^{2M} \leq c_1 \nu F^{\pm} \ell^{2M-2} U^{\pm} + c_2 \ell^{2M-1} F^{\pm} U^{\pm} U^{\mp} . \tag{C10}$$

By using (C7), in the limit $Gr_{\pm} \to \infty$, (C10) becomes

$$Gr_{\pm} \leq c \, (Re_{\pm} + Re_{\pm} Re_{\mp}) . \tag{C11}$$

[1] U. Frisch, *Turbulence: The Legacy of A. N. Kolmogorov* (Cambridge University Press, Cambridge, 1995).

[2] R. Kerr, J. Fluid Mech. **153**, 31 (1985).

[3] C. Meneveau and K. R. Sreenivasan, J. Fluid Mech. **224**, 429 (1991).

[4] K. R. Sreenivasan and R. A. Antonia, Ann. Rev. Fluids Mech. **29**, 435 (1997).

[5] G. Boffetta, A. Mazzino, and A. Vulpiani, J. Phys. A: Mathematical and Theoretical **41**, 363001 (2008).

[6] A. Arneodo, R. Benzi, J. Berg, L. Biferale, E. Bodenschatz, A. Busse, E. Calzavarini, B. Castaing, M. Cencini, L. Chevillard, et al., Phys. Rev. Lett. **100**, 254504 (2008).

[7] D. Donzis, P. Yeung, and K. Sreenivasan, Phys. Fluids **20**, 045108 (2008).

[8] T. Ishihara, T. Gotoh, and Y. Kaneda, Annu. Rev. Fluid Mech. **41**, 16 (2009).

[9] R. Pandit, P. Perlekar, and S. S. Ray, Pramana, Journal of Physics **73**, 157 (2009).

[10] S. Bramwell, P. Holdsworth, and J. Pinton, Nature **396**, 552 (1998).

[11] D. Sornette, Springer-Verlag Berlin Heidelberg (2006).

[12] D. Biskamp and W.-C. Müller, Phys. Plasmas **7**, 4889 (2000).

[13] W.-C. Müller and D. Biskamp, Phys. Rev. Lett. **84**, 475 (2000).

[14] P. D. Mininni and A. Pouquet, Phys. Rev. Lett. **99**, 254502 (2007).

[15] P. D. Mininni and A. Pouquet, Phys. Rev. E **80**, 025401 (2009).

[16] G. Sahoo, P. Perlekar, and R. Pandit, New J. Physics **13**, 013036 (2011).

[17] G. Poletto and S. T. Suess, *The Sun and the Heliosphere as an Integrated System*, vol. 317 (Springer Science & Business Media, 2013).

[18] A. N. Kolmogorov, Dokl. Akad. Nauk SSSR **32**, 16 (1941).

[19] D. Mitra and R. Pandit, Phys. Rev. Lett. **93**, 024501 (2004).

[20] S. S. Ray, D. Mitra, and R. Pandit, New J. Phys. **10**, 033003 (2008).

[21] J. Gibbon, Comm Math. Sci **10, No 1**, 131 (2011).

[22] D. Donzis, J. Gibbon, A. Gupta, R. Kerr, R. Pandit, and D. Vincenzi, J. Fluid Mech. **732**, 316 (2013).

[23] J. Gibbon, D. Donzis, A. Gupta, R. Kerr, R. Pandit, and D. Vincenzi, Nonlinearity **27**, 2605 (2014).

[24] H. Politano, T. Gomez, and A. Pouquet, Phys. Rev. E **68**, 026315 (2003).

[25] A. Basu, A. Naji, and R. Pandit, Phys. Rev. E **89**, 012117 (2014).

[26] P. S. Iroshnikov, Sov. Astron. **7**, 566 (1963).

[27] R. H. Kraichnan, Phys. Fluids **8**, 1385 (1965).

[28] R. Grauer, J. Krug, and C. Mariani, Phys. Lett. A **195**, 335 (1994).

[29] H. Politano and A. Pouquet, Phys. Rev. E **52**, 636 (1995).

[30] H. Politano, V. Carbone, and A. Pouquet, Europhys. Lett. **43**, 516 (1998).

[31] W. C. Müller, D. Biskamp, and R. Grappin, Phys. Rev. E **67**, 066302 (2003).

[32] S. Servidio, W. H. Matthaeus, and P. Dmitruk, Phys. Rev. Lett **100**, 095005 (2008).

[33] W. H. Matthaeus, A. Pouquet, P. D. Mininni, P. Dmitruk, and B. Breech, Phys. Rev. Lett **100**, 085003 (2008).

[34] J. E. Stawarz, A. Pouquet, and M.-E. Brachet, Phys. Rev. E **86**, 036307 (2012).

[35] B. Bigot, S. Galtier, and H. Politano, Phys. Rev. E **78**, 066301 (2008).

[36] H. Homann, Y. Ponty, G. Krstulovic, and R. Grauer, New J. Phys. **16**, 075014 (2014).

[37] G. Krstulovic, M.-E. Brachet, and A. Pouquet, Phys. Rev. E **89**, 043017 (2014).

[38] C. R. Doering and C. Foias, J. Fluid Mech. **467**, 289 (2002).

[39] J. D. Gibbon, ArXiv:1506.03060v3 (2015).

[40] C. R. Doering and J. D. Gibbon, Physica D **165**, 163 (2002).

[41] A. Pouquet, P. Sulem, and M. Meneguzzi, Physics of Fluids (1958-1988) **31**, 2635 (1988).

[42] S. Galtier, S. Nazarenko, A. Newell, and A. Pouquet, J. Plasma Phys. **63**, 447 (2000).

[43] M. Nelkin, Phys. Rev. A **42**, 7226 (1990).

[44] J. Schumacher, K. R. Sreenivasan, and V. Yakhot, New J. Phys. **9**, 89 (2007).

[45] S. Chakraborty, U. Frisch, W. Pauls, and S. S. Ray, Phys. Rev. E **85**, 015301(R) (2012).

[46] J. Gibbon, J. Math. Phys. **53**, 115608 (2012).

[47] A. Pouquet, in V^{th} *European School in Astrophysics, San Miniato; Lecture Notes in Physics "Plasma Astrophysics" vol. 468*, edited by C. Chiuderi and G. Einaudi (Springer–Verlag, 1996), pp. 163–212.

[48] S. Servidio, W. H. Matthaeus, M. A. Shay, P. A. Cassak, and P. Dmitruk, Phys. Rev. Lett **102**, 115003 (2009).

[49] At $m = 1$, we have equality with $c_1 = 1$. The case $m = \infty$ needs a logarithmic correction.

[50] The simple Hölder inequality $\Omega_1^\pm \leq \Omega_m^\pm$ translates to $D_1^{\pm\alpha_m/2} \leq D_m^\pm$ which, in turn, implies that the lower bound $D_1^{\pm\alpha_m/2}$ is equivalent to $\lambda^\pm = 1$.

[51] For technical reasons [40], an additive term should be included in both the denominator and numerator in (44) to take account of the forcing term in (36), but as this makes a negligible contribution it will be dropped.

[52] As a check we note that if $\chi_{m,\lambda}^+ = \chi_{m,\lambda}^- = m\lambda + 1 - \lambda$, as it does in the pure $3D$ Navier-Stokes case [23], then the sum of the exponents on the right hand side of (45) is $\frac{1}{2}\lambda$, as it should.